



Optimization of methyl orange decolorization by bismuth(0)-doped hydroxyapatite/reduced graphene oxide composite using RSM-CCD

Umit Ecer¹ · Sakir Yilmaz^{1,2} · Berdan Ulas^{1,2} · Serap Koc³

Received: 12 February 2024 / Accepted: 18 April 2024
© The Author(s) 2024

Abstract

In the current study, the catalyst for the decolorization of methyl orange (MO) was developed HAp-rGO by the aqueous precipitation approach. Then, bismuth(0) nanoparticles (Bi NPs), which expect to show high activity, were reduced on the surface of the support material (HAp-rGO). The obtained catalyst was characterized by scanning electron microscopy (SEM), energy-dispersive X-ray analysis (EDX), X-ray diffraction (XRD), and X-ray photoelectron spectroscopy (XPS) techniques. The parameters that remarkably affect the decolorization process (such as time, initial dye concentration, NaBH₄ amount, and catalyst amount) have been examined by response surface methodology (RSM), an optimization method that has acquired increasing significance in recent years. In the decolorization of MO, the optimum conditions were identified as 2.91 min, Co: 18.85 mg/L, NaBH₄ amount: 18.35 mM, and Bi/HAp-rGO dosage: 2.12 mg/mL with MO decolorization efficiency of 99.60%. The decolorization process of MO with Bi/HAp-rGO was examined in detail kinetically and thermodynamically. Additionally, the possible decolorization mechanism was clarified. The present work provides a new insight into the use of the optimization process for both the effective usage of Bi/HAp-rGO and the catalytic reduction of dyes.

Keywords Bismuth · Decolorization · Methyl orange · Hydroxyapatite · Reduced graphene oxide

Introduction

The primary causes of severe, irreversible environmental damage are indiscriminate urbanization, industrialization, and rapid population growth. Every day, numerous millions of gallons of wastewater are released by industries that produce textiles, refineries, paper pulp, pesticides, batteries, and other products. The terrestrial and aquatic natural environment's bodies, including rivers, ponds, and lakes, are endangered by the organic pollutants found in effluent.

Complicated molecules and organic dyes are used in the printing, tannery, paint, textile, and plastics industries. Presently, over 10 million distinct dyes are produced annually throughout the world (Sen et al. 2011). Because they are not completely fixed, 12–15% of the dyes used in manufacturing processes are released into the effluent (Al-Amrani et al. 2014). Due to the abovementioned problems, scientists have directed their research towards the treatment of organic pollutants in industrial wastewater and the development of innovative treatment methods. Among the treatment techniques for dye-contaminated water, methods such as coagulation (Liu et al. 2022), ion exchange (Joseph et al. 2020), adsorption (Zolfaghari et al. 2023), electrochemical treatment (Bustos-Terrones et al. 2021), flocculation (Januário et al. 2021), and chemical reduction (Truong et al. 2024) have been used recently.

Various studies have been reported examining the degradation of dyes by various reducing agents (Acar et al. 2023; Joseph and Mathew 2015; Osunlaja et al. 2012). The degradation of methyl orange (MO) in the presence of different reducing agents has been studied by many scientists. It is a known fact that reducing agents add electrons or donate hydrogen to the substrate. It should

Responsible Editor: George Z. Kyzas

✉ Umit Ecer
umitecer@gmail.com

¹ Department of Chemical Engineering, Institute of Natural and Applied Sciences, Van Yuzuncu Yil University, 65080 Van, Turkey

² Department of Mining Engineering, Faculty of Engineering, Van Yuzuncu Yil University, Van 65000, Turkey

³ Department of Mechanical Engineering, Faculty of Engineering, Van Yuzuncu Yil University, Van 65000, Turkey

be noted that the reducing agent itself is oxidized during the reduction process (Patel et al. 2022). In the current study, sodium borohydride (NaBH_4) was chosen as the reducing agent due to its unique ability to reduce imine and carbonyl functional groups to amines and alcohols, respectively. The reaction rate in the decolorization reaction is significantly influenced by the choice of catalyst. Recently, metal nanoparticles (MNPs) have gained attention as catalysts because of their special characteristics. Despite their seeming uniqueness, MNPs tend to collect in clusters because of their high surface energy, which lowers catalytic activity and causes long-term stability issues. A large surface area supporting material can be used to solve the MNP agglomeration problem. To produce MNPs with a controlled size and distribution that are both stable and active, it is important to choose the right support (Ecer et al. 2023). MNPs (Pd, Pt, Ag, Bi, Ni, Co, Cu, etc.) have been extensively investigated because of their mechanical, catalytic, and electrochemical qualities in a variety of fields. Bismuth nanoparticles (Bi NPs) are one type of metal-based catalyst that has intriguing properties for the degradation of pollutants in water. Compounds based on Bi NPs and their composites have a variety of useful uses, such as energy storage, gas sensors, and catalysts. These substances are well known for their low cost, good dielectric qualities, high oxygen conductivity, and non-toxicity (Alovn et al. 2023). However, because of their small size and high surface energy, metal nanoparticles are prone to aggregation, which will decrease their catalytic activity. Moreover, it is challenging to recover and recycle Bi NPs from the aquatic system, which can lead to secondary contamination and restrict their practical uses (Ecer and Yilmaz 2024). Supporting materials have been utilized to immobilize NPs onto solid supports to address such issues. These materials included clay minerals, biochar, silica gel, activated carbon, polymers, and magnetic materials (Khan et al. 2023; Xue et al. 2023).

Graphene oxide (GO), a kind of 2-D nanostructured sp^2 carbon material, has garnered a lot of attention because of its remarkable qualities, which include high optical transparency, great electrical conductivity, and a vast surface area. Utilizing the graphene nanosheet as an ideal conductive platform for nanoparticles to create hybrid nanocomposites is therefore highly promising. Additionally, it is verified that the graphene nanosheet can stop nanoparticle aggregation (Ding et al. 2021). Compared to GO, reduced graphene oxide (rGO), a chemically altered form of GO, is more economically suitable for large-scale manufacturing. rGO is widely used in the synthesis of GO-based composites. rGO exhibits higher surface area, higher electrical conductivity, superior electrocatalytic properties, and more efficient carrier mobility than GO (Liu et al. 2018; Wei et al. 2017). Additionally,

rGO enhances cellular behavior due to its biocompatibility and the presence of a small number of functional groups in its basal plane and edges, including hydroxyl, epoxy, carboxyl, and carbonyl. These groups enable the creation of bioactive nanomaterials with customized microstructures and enhanced mechanical properties. Hydroxyapatite (HAp) is one of the major common forms of ceramic biomaterials. Bio-ceramics are an example component of HAp with carbon (C) nanotubes that have only recently been studied. Because of its excellent biological properties, biocompatibility, biomedical application properties, and bioactive, it is the primary constituent of mammalian hard tissues (tooth and bone); it was also employed for a variety of medical applications. $\text{Ca}_{10}(\text{PO}_4)_6(\text{OH})_2$ is the main chemical compound with the chemical formula of pure HAp. Pure HAp has a Ca:P atomic ratio of 1.67, indicating large stability and calcium orthophosphates have molecular ratios ranging from 2 to 0.5 (Ciobanu et al. 2015; Ciobanu and Harja 2019). Combining HAp and reduced graphene oxide (rGO) can create a material with several advantages. As a result of doping, the material's properties such as mechanical, electrical, surface properties and biocompatibility can be improved, making it more effective in various biomedical and material science applications. In particular, the mechanical biocompatibility and performance of HAp can be developed seriously by reinforcement with rGO (Lee et al. 2015).

To maximize the benefits of a system, process, or product, it is necessary to optimize its performance. Finding the optimum conditions to apply a process that yields the best outcome is commonly referred to as optimization. Traditionally, optimization has been done by tracking the impact of a single factor on an experimental response one at a time. Only one parameter is altered; the values of the others remain unchanged. The main drawback of this approach is that it ignores the interactions between the variables under investigation. Consequently, this method does not fully illustrate how the parameter affects the response (Hanrahan and Lu 2006). The increased number of experiments required to carry out the research, which increases time and costs as well as the consumption of reagents and materials, is another drawback of one-factor optimization. Multivariate statistical techniques have been used to optimize analytical procedures to solve this issue (Bezerra et al. 2008). Response surface methodology (RSM) is one of the most pertinent multivariate techniques used in analytical optimization. The goal of response surface methodology is to make statistical predictions by describing the behavior of a data set using a set of mathematical and statistical techniques based on the fit of a polynomial equation to the experimental data. It works well when many factors influence a response or a group of relevant responses. To achieve optimal system

performance, the goal is to concurrently optimize the levels of these variables (Bezerra et al. 2008; Hanrahan and Lu 2006).

In the current work, HAp-rGO was first produced using the aqueous precipitation method to develop the catalyst that would be used in the decolorization process. Then, using the NaBH₄ reduction method, bismuth(0) nanoparticles (NP), which we anticipate to exhibit high activity, were deposited on the surface of the support material (HAp-rGO). RSM was used to model the optimization of the key parameters influencing the decolorization of MO (time, MO concentration, NaBH₄ amount, and catalyst amount). Maximum decolorization efficiency (%) was then calculated by identifying the parameters optimum points using the resulting model equation. Scanning electron microscopy (SEM), energy-dispersive X-ray analysis (EDX), X-ray diffraction (XRD), and X-ray photoelectron spectroscopy (XPS) analyses were conducted to elucidate the surface properties of the obtained catalyst. Additionally, the decolorization of MO using the Bi/HAp-rGO was examined in terms of thermodynamics and kinetics. Furthermore, the possible mechanism of decolorization was clarified. The current study offers a fresh viewpoint on the use of the optimization procedure for the catalytic reduction of dyes as well as the efficient utilization of Bi/HAp-rGO.

Material and methods

Pure HAp and HAp-rGO (rGO, purity %99, S.A 15.62 m²/g, 2–5 layers, nanografi) composite were synthesized by an aqueous precipitation method [1]. Calcium nitrate tetrahydrate (Ca(NO₃)₂·4H₂O), di-ammonium hydrogen phosphate ((NH₄)₂HPO₄), rGO (wt% 5) were used as starting reagents. To prepare the pure and doped samples, Ca(NO₃)₂·4H₂O (solution 1) and (NH₄)₂HPO₄ (solution 2) were added into distilled water to prepare the solutions with a certain molar ratio. These two powders were dissolved separately in distilled water with a Ca/P ratio of 1.67. Ammonia (NH₄OH) was added into (NH₄)₂HPO₄ solution after previous solutions were stirred for 1 h. NH₄OH was added to both solutions to bring the pH level to 11–12. Different from pure HAp, rGO was added at the same time into the solution in a dropwise manner after stirring for 10 min. The final mixture was heated until boiling to increase the reaction. After boiling, the mixture was left for stirring for 24 h. After 1 day of aging, the solution was filtered to obtain a wet cake. The wet cake was dried in an oven at 200 °C to remove the excess water and ammonia. The precipitated and dried HAPs were crushed with an agate mortar and pestle, and the resulting powder and bulks were sintered at 1100 °C for 1 h (Gungor Koc 2019; Song et al. 2001).

To obtain the bismuth(0)-doped catalyst, the NaBH₄ reduction method was used. Typically, a certain amount of HAp-rGO and bismuth(III) subnitrate (Bi₅O(OH)₉(NO₃)₄) was dispersed in 20 mL of ultra-pure water. The solution was mixed for 2 h. Then, NaBH₄ was added dropwise to the above mixture, followed by stirring for another 1 h. After reaction completion, the obtained material was filtered and washed with ultra-pure water several times. Finally, it was dried in an oven at 70 °C overnight. The synthesis procedure is given schematically in Fig. 1.

RSM-CCD-based catalytic reduction of MO

The decolorization of MO in the presence of NaBH₄ was selected to investigate the catalytic activity of Bi/HAp-rGO. All the catalytic tests were achieved in a flask in which the volume of the solution was 5 mL and achieved under different conditions including time (min), MO concentration (C_o, mg/L), NaBH₄ amount (mM), and catalyst dosage (mg/mL). The detailed experimental conditions for the decolorization of MO are given in Table 1. The MO concentration after and before decolorization was measured using UV–Vis spectroscopy at λ_{max} = 464 nm. The decolorization efficiency (%) was calculated by Eq. 1.

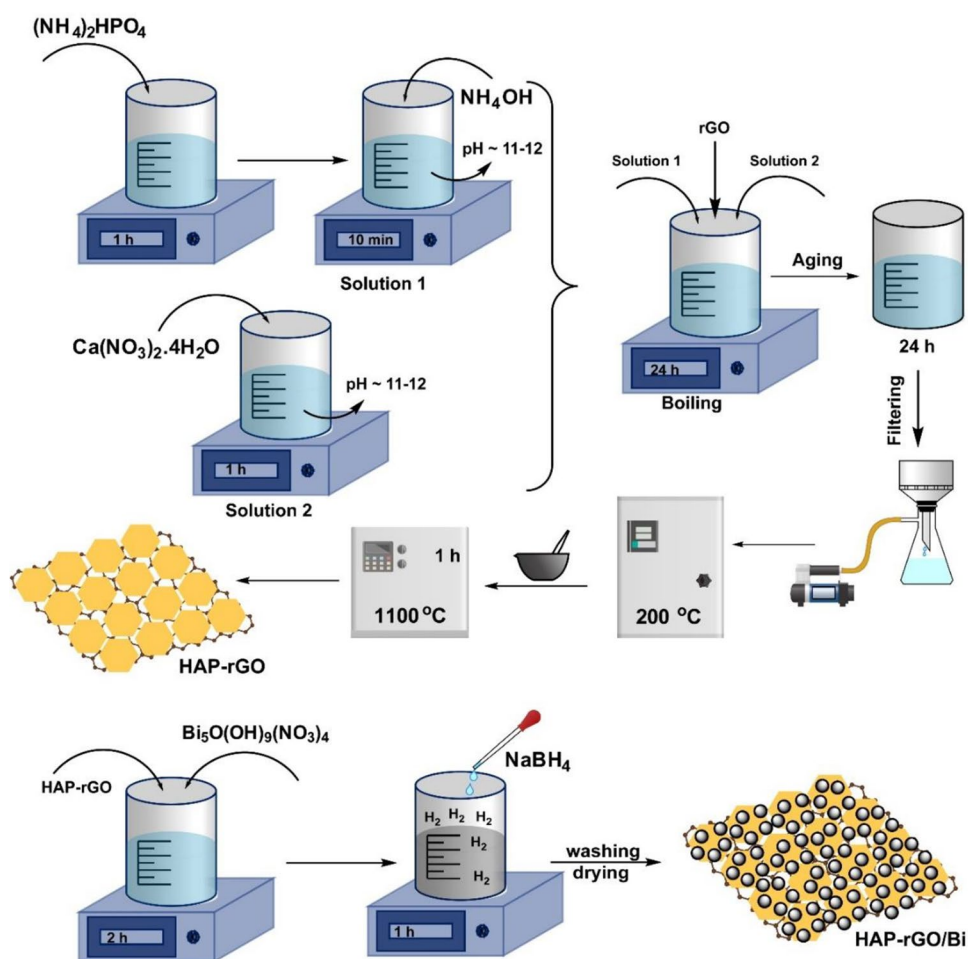
$$\text{Decolorization efficiency (\%)} = \frac{(C_o - C_e)}{C_o} \times 100 \quad (1)$$

The experimental design ensures simultaneous optimization of coefficients that affect the response, besides development performance features and minimizing errors with few tests. The RSM-CCD matrix was used to investigate and optimize the decolorization efficiency (%) of MO as a function of the parameters: time (min), MO concentration (C_o, mg/L), NaBH₄ amount (mM), and catalyst dosage (mg/mL). The total number of experiments was determined with the 2^k + 2k + 6 equation (where k is the number of independent parameters). The six repetitions at the center point were performed to minimize experimental errors. A total of 30 experiments for the four parameters were performed to obtain decolorization efficiency (Table 1). The response for the optimization procedure can be acquired as quadratic or linear equations. The relation between the response and independent parameters can be given as the following equation.

$$y_p = \beta_o + \sum_{i=1}^k \beta_i x_i + \sum_{i=1}^k \beta_{ii} x_i^2 + \sum_{i=1}^k \sum_{j=i+1}^k \beta_{ij} x_i x_j \quad (2)$$

where y_p is the response (decolorization efficiency); x_i and x_j are the independent variables; and β_o, β_i, β_{ii}, and β_{ij} are constant, linear, square, and interaction effect of the model,

Fig. 1 Schematic representation of Bi/HAp-rGO synthesis



respectively. To confirm the suggested model's statistical significance and practicality, analysis of variance (ANOVA) was employed. The significance of every parameter and the fit of the proposed model were explained by analyzing the correlation coefficient (R^2), Fisher value (F -value), and probability value (p -value).

Results and discussion

Characterization

The surface morphology, elemental distribution on the surface, crystallographic properties, and oxidation state of Bi/HAp-rGO were investigated by SEM–EDX, elemental mapping, XRD, and XPS analysis.

Figure 2 depicts the XRD pattern of Bi/HAp-rGO. The 10–40° and 40–60° 2θ ranges are magnified and shown in Fig. 2B, C. As can be clearly seen from Fig. 2B, C, almost all characteristic peaks of HAp are observed. The diffraction peaks observed at 25.9°, 31.1°, 31.9°, 32.9°,

34.4°, 39.8°, 46.7°, 49.5°, 50.5°, and 53.0° 2θ angles correspond to the reflection of the (002), (211), (112), (300), (202), (310), (222), (213), (321), and (004) planes of HAp, respectively (JCPDS card No: 09–432) (Rogina et al. 2013). Other characteristic peaks of HAp are labeled in Fig. 2B, C. Also, the peak at about 42.3° 2θ angle is attributed to the (101) facet of rGO (JCPDS card No: 41–1487) (Topçu and Dağcı Kıranşan 2019). The diffraction peaks detected at 22.6°, 27.3°, 38.1°, 39.7°, and 48.2° 2θ angles were attributed to the reflections of hexagonal Bi (003), Bi (012), Bi (104), Bi (110), and Bi (202) planes, respectively (JCPDS 86–1330) (Wang et al. 2007). As a result, almost all characteristic peaks of HAp, rGO, and Bi were observed, and it was concluded that Bi/HAp-rGO was successfully synthesized.

SEM images and corresponding EDX spectra of HAp, HAp-rGO, and Bi/HAp-rGO are shown in Fig. 3. Figure 3a shows a conventional image of HAp that can be verified from the literature. The presence of P and Ca in the HAp structure was detected from the EDX spectrum. Although no significant changes are observed in the SEM images of

Table 1 CCD design matrix and results

Parameters	Units	Range and level				Decolorization efficiency, %
		-1	0	1		
Time	min	0.5	2.75	5		
C _o	mg/L	5	27.5	50		
NaBH ₄ amount	mM	1	15.5	30		
Catalyst amount	mg/mL	0.5	2.75	5		
Run	A	B	C	D		
1	0.5	50	1	0.5	25.60	
2	2.75	27.5	30	2.75	98.04	
3	0.5	50	30	5	83.60	
4	2.75	27.5	15.5	2.75	98.58	
5	0.5	50	30	0.5	60.82	
6	2.75	27.5	15.5	2.75	97.75	
7	5	5	30	0.5	95.20	
8	5	50	1	5	75.80	
9	2.75	27.5	15.5	0.5	82.66	
10	0.5	50	1	5	67.60	
11	5	5	1	0.5	86.80	
12	2.75	27.5	1	2.75	72.55	
13	2.75	27.5	15.5	2.75	98.29	
14	5	27.5	15.5	2.75	96.76	
15	5	50	30	5	89.38	
16	2.75	50	15.5	2.75	89.08	
17	5	5	30	5	96.60	
18	0.5	5	1	5	79.20	
19	5	50	30	0.5	75.72	
20	0.5	27.5	15.5	2.75	79.67	
21	5	5	1	5	91.40	
22	2.75	27.5	15.5	5	98.15	
23	2.75	27.5	15.5	2.75	97.96	
24	0.5	5	1	0.5	73.60	
25	2.75	5	15.5	2.75	97.40	
26	5	50	1	0.5	55.80	
27	0.5	5	30	5	87.20	
28	2.75	27.5	15.5	2.75	98.40	
29	2.75	27.5	15.5	2.75	98.26	
30	0.5	5	30	0.5	87.40	

HAp-rGO, the increase in the intensity of the oxygen peak in the EDX spectrum indicates that rGO has entered the structure (Fig. 3b). Bi nanoparticles reduced on HAp-rGO can be followed in Fig. 3c. Additionally, Bi peaks were detected in the EDX spectrum of Bi/HAp-rGO. Carbon and oxygen elemental mapping images of Bi/HAp-rGO indicate that rGO has a relatively more homogeneous distribution. Phosphorus and calcium elemental mapping images show that

P and Ca in HAp are clustered in places. It was determined that the Bi distribution on HAp-rGO did not show severe agglomeration.

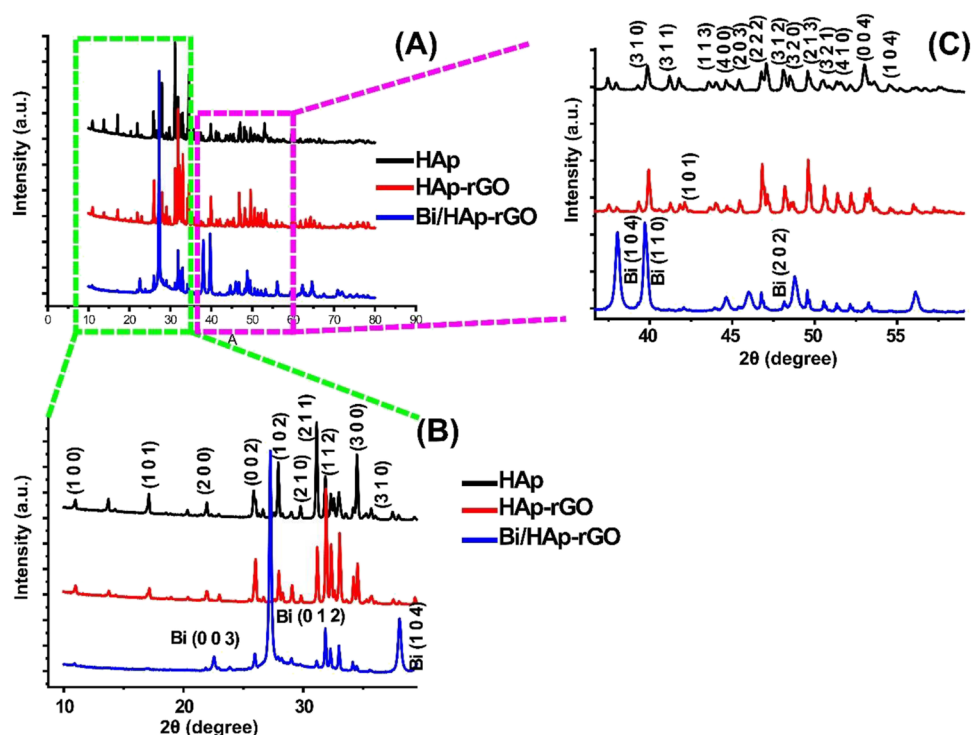
XPS analysis was performed to determine the chemical state of the Bi/HAp-rGO catalyst. Figure 4 shows the general and partial XPS survey of Bi/HAp-rGO. In the general scanning spectrum of Bi/HAp-rGO, C 1 s and O 1 s arising from rGO and P 2 s, P 2p, Ca 2p, and Ca 3p peaks from HAp were observed (El-Aal et al. 2022; Zhang et al. 2015). In addition, Bi 4p, Bi 4d, Bi 5f, and Bi 4p peaks were detected indicating the presence of Bi in the catalyst system (Fig. 4a) (Rauf et al. 2015). The peaks at 284.5 eV, 286.1 eV, and 287.7 eV BE obtained as a result of the deconvolution of the C 1 s high-resolution spectra of Bi/HAp-rGO were attributed to sp² carbon (C=C), C-O, and C=O, respectively (Qin et al. 2017). The relative C=C, C-O, and C=O ratios in the Bi/HAp-rGO structure were determined as 80.0%, 5.08%, and 14.9%, respectively. The convoluted C 1 s spectrum in Fig. 4b showed high compatibility with the spectra of rGOs reported in the literature (Johra and Jung 2015; Sharma et al. 2019). Bi 4f high-resolution spectra of Bi/HAp-rGO are given in Fig. 4c. The doublet detected at 163.7 eV and 158.5 eV BE was attributed to the presence of Bi 4f_{5/2} and Bi 4f_{7/2}, respectively (Lu et al. 2019). From the Bi 4f core level spectra, it was seen that Bi in the Bi/HAp-rGO structure was in its elemental state. The absence of any oxide of Bi in the structure indicates that the Bi salt was successfully reduced in its elemental state onto HAp-rGO, and the XPS results support the XRD results in this respect.

Statistical analysis based on RSM for MO decolorization

CCD in RSM was applied to evaluate the effects of the process parameters on the decolorization of MO via Bi/HAp-rGO in the existence of NaBH₄. Four different parameters in three levels (-1, 0, +1)—time (A, min), MO concentration (C_o) (B, mg/L), NaBH₄ amount (C, mM), and catalyst dosage (D, mg/mL)—were tested for the selected response (the decolorization of MO, %). The obtained results are tabulated in Table 1.

A quadratic polynomial model expressing the relationship between the selected independent parameters and the response was presented in Eq. 2. ANOVA results for MO decolorization are represented in Table 2. It was reported that very high *F*-value and very low *p*-value (*p* < 0.05) were statistically significant for each parameter (Sharma et al. 2023; Zolfaghari et al. 2023). The low *p*-value of 0.0001 for the obtained model indicates that it is statistically significant. The significant model terms for MO decolorization were A, B, C, D, BC, BD, A², and C². Moreover, *R*² value (*R*² = 0.96) for MO decolorization is extremely high, indicating the applicability and adequacy of the created model.

Fig. 2 XRD pattern of Bi/HAp-rGO. **A** The entire spectrum. **B** 2θ range of $10\text{--}40^\circ$. **C** 2θ range of $40\text{--}60^\circ$



$$\begin{aligned}
 \text{The decolorization of MO}(\%) = & +62.55557 + 10.62281[\text{Time}] - 0.82231[C_o] \\
 & + 1.92283[\text{NaBH}_4 \text{ amount}] + 6.27541[\text{Catalyst dosage}] + 0.020346[\text{Time}][C_o] \\
 & - 0.049655[\text{Time}][\text{NaBH}_4 \text{ amount}] - 0.37679[\text{Time}][\text{Catalyst dosage}] \\
 & + 9.44828E - 003[C_o][\text{NaBH}_4 \text{ amount}] + 0.10746[C_o][\text{Catalyst dosage}] \\
 & - 0.066207[\text{NaBH}_4 \text{ amount}][\text{Catalyst dosage}] - 1.17161[\text{Time}]^2 - 1.79649E - 003[C_o]^2 \\
 & - 0.042133[\text{NaBH}_4 \text{ amount}]^2 - 0.74064[\text{Catalyst dosage}]^2
 \end{aligned} \quad (3)$$

The plot of the estimated responses by the model versus actual responses is demonstrated in Fig. 5a. As seen in Fig. 5a, the data is normally distributed on a straight line, confirming the model's unique ability to predict experimental data. On the other hand, a normal probability plot of the residuals is given in Fig. 5b. From Fig. 5b, the residuals are dispersed around a straight line. This statistical analysis shows that the model is applicable. According to the ANOVA results and Fig. 5, it can be said that the suggested model is valid for the system.

3D RSM plots to investigate the effects of each independent parameter and determine the optimal conditions for maximum response were generated in Fig. 6. The reaction time shows a noticeable effect in the decolorization efficiency of MO dye. With an increase in reaction time, more decolorization was obtained. The decolorization efficiency of MO due to the increase in reaction time is seen in Fig. 6a, b. This is due to the reaction time between the synthesized catalyst and MO dye affecting the saturation state of the Bi/HAp-rGO surface. With the increase of reaction time, MO molecules will interact more with the reaction sites on the

catalyst surface, resulting in increased decolorization efficiency of MO (Al-Ansari et al. 2024; Zhou et al. 2024). It was observed that the maximum decolorization efficiency of MO reached its maximum in about 3 min and did not show a significant increase at later levels. Figure 6a, c shows the effect of C_o on the MO decolorization efficiency. The results revealed that increasing the concentration of MO dye from 5 to about 19 mg/L partially increased the MO decolorization efficiency. It was observed that the decolorization efficiency gradually decreased at higher concentrations. The positive effect on decolorization efficiency observed at low C_o values is initially attributed to the fact that fewer MO molecules move freely to more active sites on Bi/HAp-rGO (Shrivastava et al. 2024). In addition, the decrease in decolorization efficiency at high levels indicates that more MO molecules block the active sites of the catalyst, and therefore, the efficiency decreases due to the competition of more MO dyes on the catalyst surface (Roy et al. 2023; Shrivastava et al. 2024). Moreover, the MO and BH_4^- ions on the surface of Bi/HAp-rGO were adsorbed, based on the Langmuir-Hinshelwood process. This is a reversible process that creates

Fig. 3 SEM images and corresponding EDX spectrum of **a** HAp, **b** HAp-rGO, and **c** Bi/HAp-rGO. Elemental mapping analysis of Bi/HAp-rGO for **d** overlay, **e** carbon, **f** oxygen, **g** phosphorus, **h** calcium, and **i** bismuth

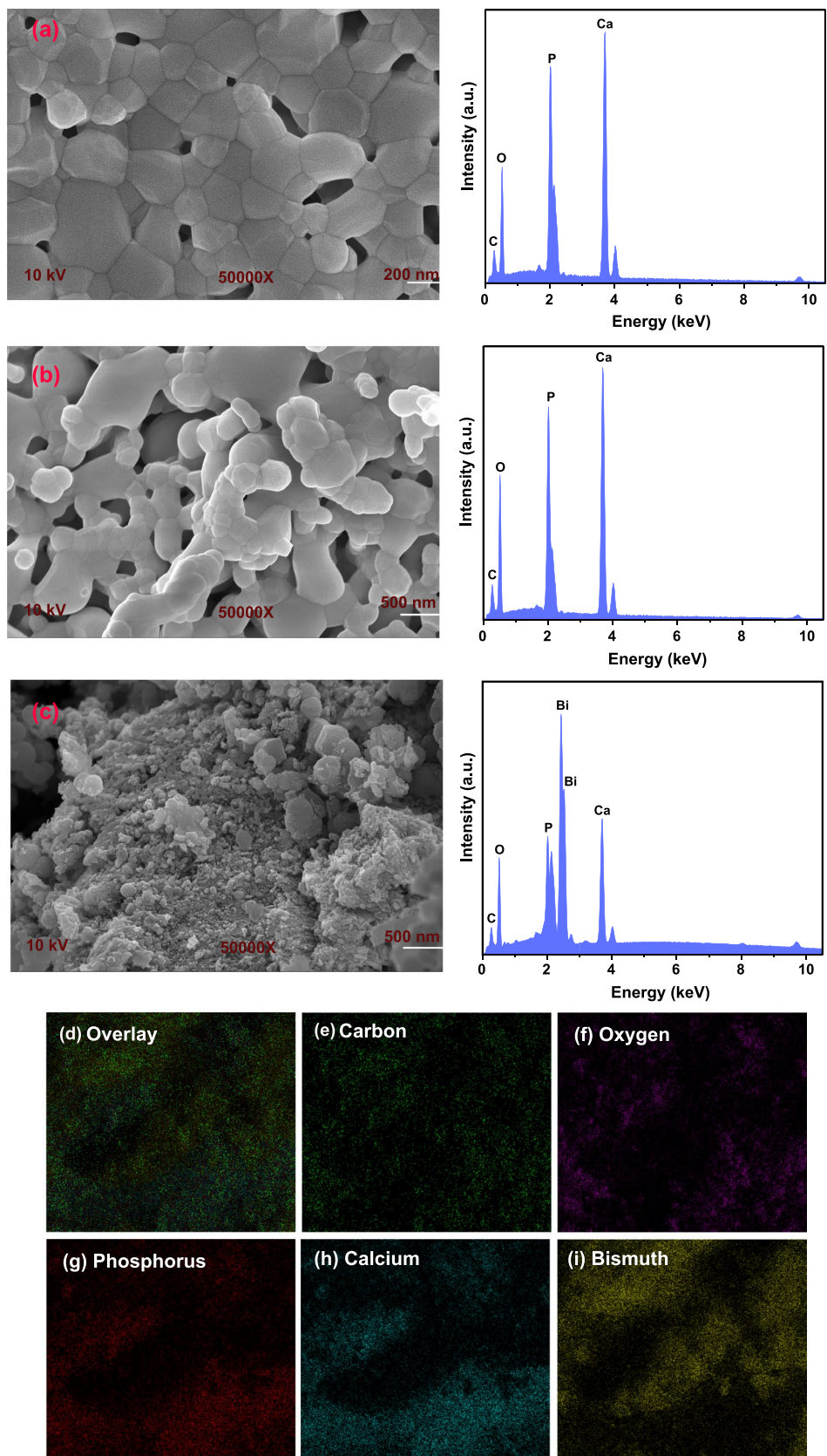


Fig. 4 a General survey, b C 1 s, and c Bi 4f core level XPS spectra of Bi/HAp-rGO

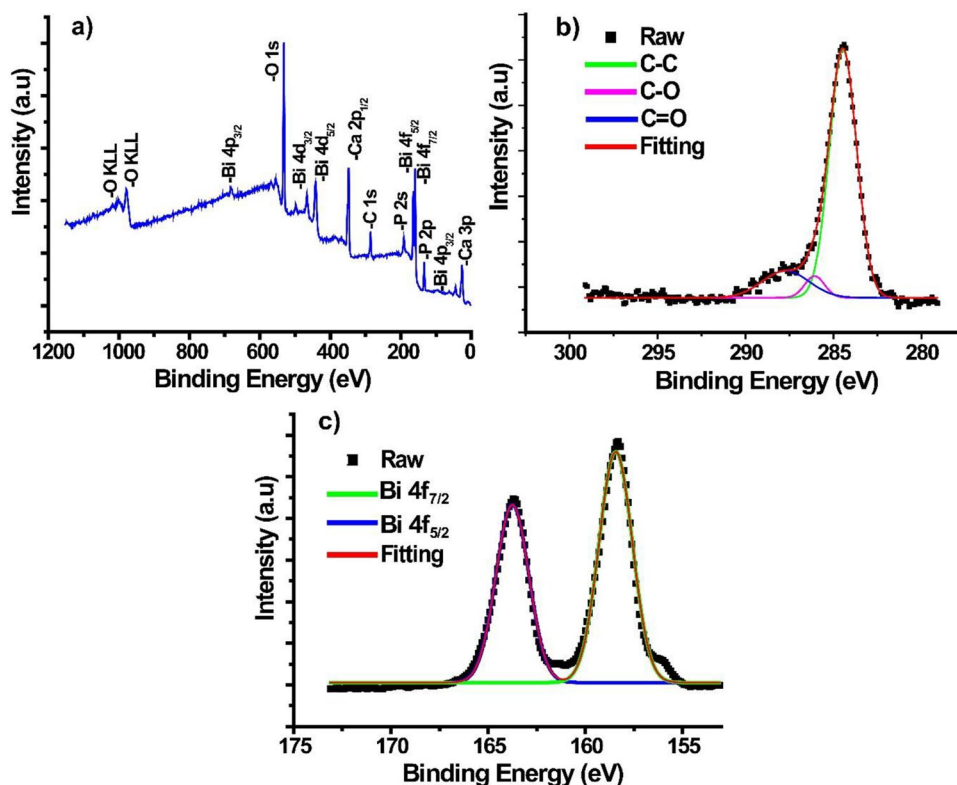


Table 2 ANOVA results

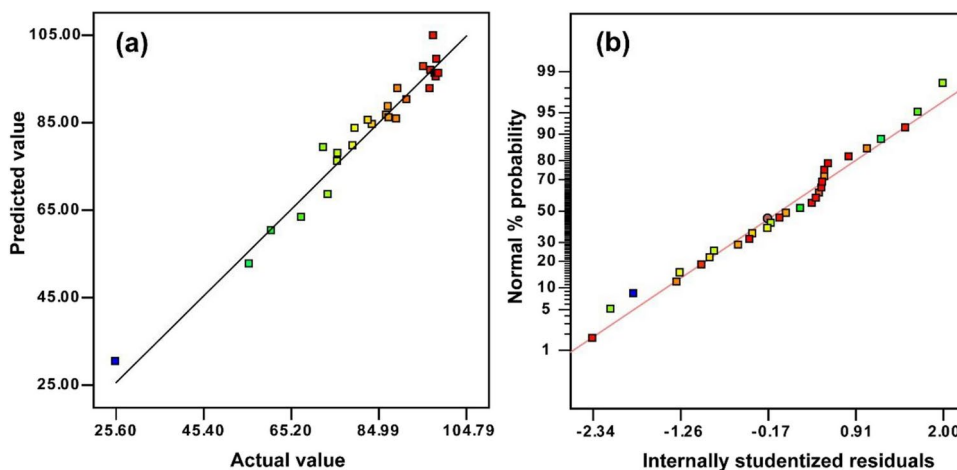
Source	Sum of squares	df	Mean square	F-value	p-value	
Model	7507.75	14	536.27	27.76	<0.0001	Significant
A-Time	783.70	1	783.70	40.57	<0.0001	
B-C ₀	1632.11	1	1632.11	84.50	<0.0001	
C-NaBH ₄ amount	1177.92	1	1177.92	60.98	<0.0001	
D-Catalyst dosage	872.66	1	872.66	45.18	<0.0001	
AB	16.97	1	16.97	0.88	0.3634	
AC	41.99	1	41.99	2.17	0.1610	
AD	58.22	1	58.22	3.01	0.1030	
BC	152.03	1	152.03	7.87	0.0133	
BD	473.50	1	473.50	24.51	0.0002	
CD	74.65	1	74.65	3.86	0.0681	
A ²	91.15	1	91.15	4.72	0.0463	
B ²	2.14	1	2.14	0.11	0.7437	
C ²	203.32	1	203.32	10.53	0.0054	
D ²	36.42	1	36.42	1.89	0.1899	
R ² =0.9628						

competition between both MO and BH₄⁻ for the active sites of Bi/HAp-rGO (Anwar et al. 2021). For this reason, it can be stated that a high concentration of MO may reduce the yield by slowing down the reaction rate.

The amount of NaBH₄ was varied within the range of 1 to 30 mM to explore the impact on the decolorization activity. Figure 6b, d shows that the effect of the amount

of NaBH₄ on the decolorization efficiency increased up to about 20 mM beyond which a gradual decrease was noticed due to the increase in NaBH₄ amount. As the amount of NaBH₄, a strong reducing agent, increased, more hydrogen was produced and bound to the catalyst and the decolorization efficiency of the dye increased. This can be attributed to BH₄⁻ ions as a result of the ionization of NaBH₄. Through

Fig. 5 **a** Predicted versus actual plot and **b** normal probability plot obtained for MO decolorization



the catalyst, which functions as an electron carrier, hydrogen interacts with the MO molecules, reducing them (Acar et al. 2023). Also, this suggests that electron donor BH_4^- is delivered to the catalyst and electrons are transported to acceptor MO molecules, resulting in the decolorization of the dye molecules (Alshaikhi et al. 2022). On the other hand, the use of excessive amounts of NaBH_4 prevented dye decolorization because when the catalyst amount was constant, the produced hydrogen adhered to the catalyst surface and the active sites required on the catalyst surface for the adsorption of MO molecules decreased and as a result, the efficiency was likely to decrease (Naseem et al. 2019). As displayed in Fig. 6c, d, there was a positive impact of Bi/HAp-rGO on the decolorization of MO when the catalyst dosage increased from 0.5 to 5 mg/mL, and it reached a maximum of about 3 mg/mL. However, the catalyst dosage had no significant change on the decolorization efficiency when the catalyst dosage was high enough. The increase of MO decolorization efficiency with increasing Bi/HAp-rGO dosage could be due to more available active sites, resulting in more dye to be decolorized (Saikia et al. 2017; Wang et al. 2020).

Optimization and validation stage

The decolorization of MO dye using Bi/HAp-rGO in the presence of NaBH_4 was optimized using RSM modeling via the Design-Expert program (trial version). Four major parameters (time, C_0 , NaBH_4 amount, and Bi/HAp-rGO dosage) were selected for the optimization of MO decolorization, while the decolorization efficiency of MO as response. The optimum conditions of the independent parameters and response were obtained by setting the parameters to “in range” and the responses to “maximum.” In the optimization stage, the desirability function, which ranges from 0 (unfavorable response) to 1 (favorable response), is a numerical tool used to determine the desired target for both the

independent parameters and the response (Zolfaghari et al. 2023). The optimal conditions for the decolorization of MO using Bi/HAp-rGO in the existence of NaBH_4 were determined by selecting the best desirability function by the software. The optimum points were found as time, 2.91 min; C_0 , 18.85 mg/L; NaBH_4 amount, 18.35 mM; and Bi/HAp-rGO dosage, 2.12 mg/mL. At the determined process conditions, the maximum decolorization efficiency of MO was found to be 99.60% with an overall desirability of 1. The validation of the suggested model was carried out by keeping the parameters at the obtained optimal points, and the decolorization efficiency of MO was experimentally 99.49%. The negligible difference between the experimental and predicted results indicated that the suggested model can be acceptable.

At the achieved optimal conditions, further experiments were conducted to evaluate the significance of Bi/HAp-rGO. For this purpose, the effects of HAp, HAp-rGO, only NaBH_4 , and Bi/HAp-rGO without NaBH_4 were investigated on the decolorization efficiency of MO (Fig. S1). The decolorization efficiencies of MO for HAp, HAp-rGO, only NaBH_4 , and Bi/HAp-rGO without NaBH_4 were found as 33.1%, 41.91%, 16.45%, and 18.24%, respectively, at the optimal process conditions. A slight change in the decolorization percentage of MO was observed in the absence of either NaBH_4 or catalyst. However, it was observed that the addition of both catalyst and NaBH_4 increased dye decolorization, indicating that the catalyst in the existence of NaBH_4 has a synergistic effect on the decolorization of MO (Ravikumar et al. 2016). Therefore, it clearly demonstrated that neither the catalyst nor NaBH_4 alone was suitable to finish the rapid decolorization of MO. On the other hand, the decolorization efficiency of Bi/HAp-rGO is quite high compared to HAp and HAp-rGO materials. So, it is possible to conclude that the catalyst effectively increased the decolorization of MO by transmitting electrons from BH_4^- species to MO through the Bi NPs (Saikia et al. 2017). These results

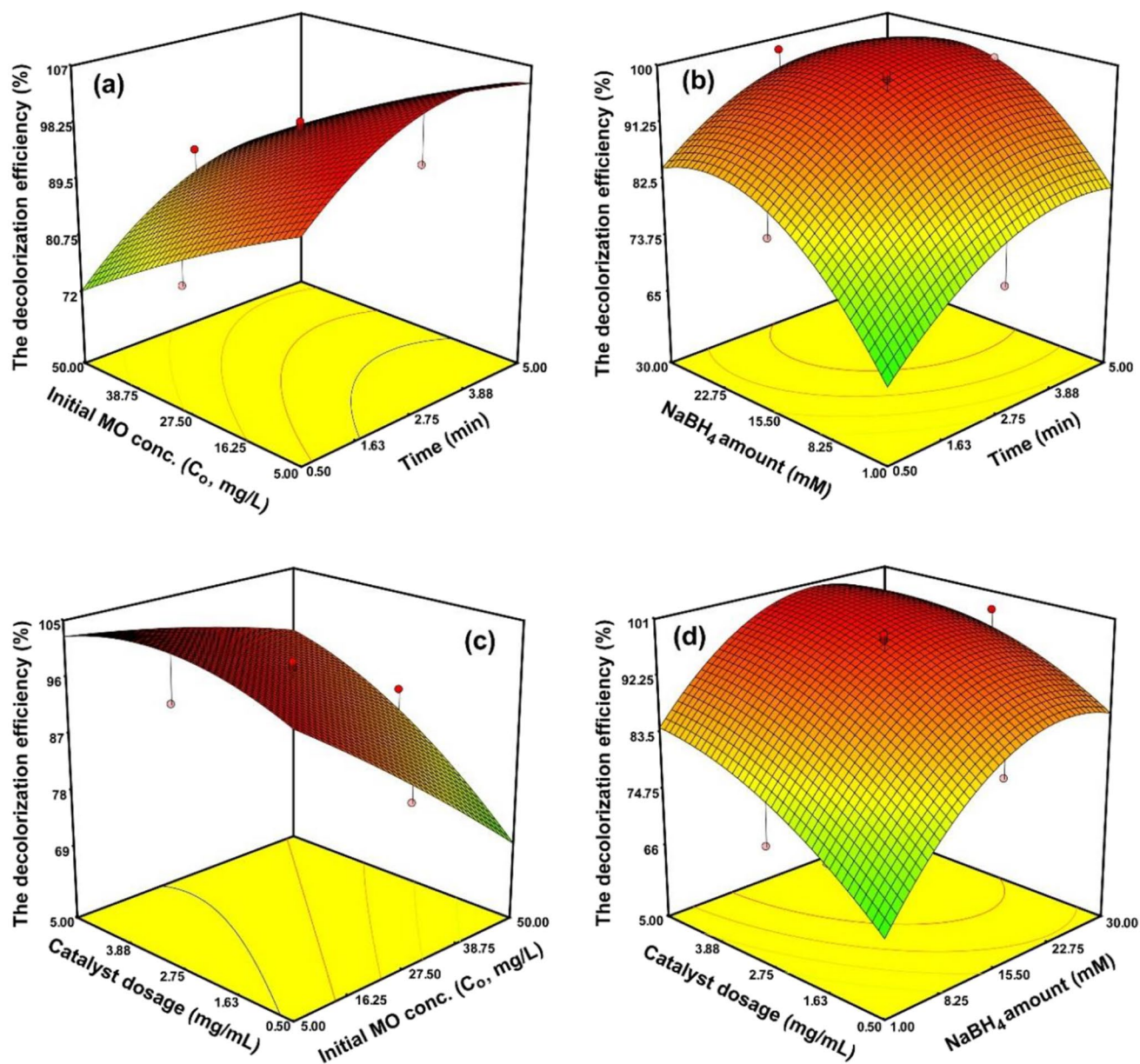


Fig. 6 3D response plots of **a** time, C_0 ; **b** time, NaBH_4 amount; **c** C_0 , catalyst dosage; and **d** NaBH_4 amount, catalyst dosage

Table 3 Comparison of various catalysts for the decolorization of MO

Catalyst	Time	C_0	NaBH_4 amount	Catalyst amount	Decolorization efficiency (%)	Ref
Pd NPs/RGO- <i>A. abrotanum</i>	140 s	10 mg/L	0.1 M	0.33 mg/mL	99	(Hashemi Salehi et al. 2019)
$\text{CoFe}_2\text{O}_4/\gamma\text{-Fe}_2\text{O}_3$	36 min	50 mg/L	0.3 M	2 mg/mL	$\geq 99.9\%$	(El-Subruiti et al. 2019)
Fe_3O_4 @Nico-Ag	12 min	10 mM	100 mM	0.33 mg/mL	~ 100	(Kurtan et al. 2016)
Pd/CNFs	240 min	10 mg/L	0.026 mM	2 mg/mL	98.9	(Najem et al. 2020)
Au/ Fe_3O_4 -chitosan	18 min	0.1 mM	0.04 M	2 mg/mL	> 90	(Liu et al. 2016)
SiO_2 -Ag CS Nps	5 min	0.0524 mM	0.001 M	0.5 mL	91.7	(Khalik et al. 2020)
Bi/HAp-rGO	2.91 min	18.85 mg/L	18.35 mM	2.12 mg/mL	99.6	This study

suggested that the Bi/HAp-rGO is effective as a catalyst in the presence of NaBH_4 for the decolorization of MO.

The catalytic activity of the Bi/HAp-rGO for the decolorization of MO was compared with various catalysts from the literature given in Table 3. By comparison, Bi/HAp-rGO demonstrated higher or similar catalytic activities compared to the various catalyst systems reported in the literature for MO decolorization. Furthermore, the present work provides a new perspective on the application of the optimization process for both the effective usage of catalysts and the catalytic reduction of dyes. This shows that the study will significantly add to the literature and can be a reference for future studies.

Kinetic and thermodynamic studies

The pseudo-first-order kinetic model could be evaluated for the decolorization of MO by Bi/HAp-rGO in the existence of the high concentration of the reducing agent (Sarkar et al. 2021). The pseudo-first rate constant (k_{app}) was calculated by using the pseudo-first-order kinetic model equation (Eq. S1). The kinetic plot of $\ln(C_0/C_t)$ vs. reaction time at different temperatures is shown in Fig. S2a. The results obtained from the kinetic model are presented in Table S1. The results showed that the k_{app} was found to increase with temperature. The Arrhenius equation (Eq. S2) can be used to compute the reaction activation energy (E_a). The value of E_a was calculated from the linear correlation slope between $\ln k$ versus $1/T$ (Fig. S2b). This value was calculated to be 6.75 kJ/mol for the decolorization of MO by Bi/HAp-rGO in the existence of NaBH_4 . The activation enthalpy (ΔH^\ddagger) and activation entropy (ΔS^\ddagger) as thermodynamic parameters for the decolorization of MO were calculated from the linear plot of $\ln k/T$ vs. $1/T$ (Fig. S2c), and the values are presented in Table S1. The ΔH^\ddagger value obtained in the case of

the decolorization of MO was 4.19 kJ/mol, indicating that there is an endothermic nature for the decolorization process due to the positive value of its. Moreover, the value of ΔS^\ddagger was found to be -223.36 J/mol K. This negative value indicated the decrease in the randomness at reaction solution interfaces via decolorization of MO, namely, lower randomness (Akl et al. 2023; Srivastava et al. 2022).

MO decolorization mechanism of Bi/HAp-rGO

The possible mechanism for the decolorization of MO under the optimal conditions using Bi/HAp-rGO catalyst is shown in Fig. 7. NaBH_4 as a reducing agent was used to the decolorization of MO molecules in aqueous settings. In general, MO aqueous solution is orange. However, in the existence of a reducing agent (NaBH_4), the MO dye molecules were turned into a colorless form (Leuco-MO). Bi NPs serve as an electron transfer mechanism for MO dye, transferring electrons from an electron donor to an electron acceptor. BH_4^- ions generated from NaBH_4 act as electron donors (nucleophilic), while MO molecules as electrophile (electron acceptor) (Mascarenhas & Varanda 2021). In the first stage, simultaneous adsorption of BH_4^- ions and MO dye onto the catalyst surface occurs. Later, electron transfer occurs between nucleophilic BH_4^- ions and the electrophilic MO molecules through Bi/HAp-rGO. Finally, the orange color MO becomes colorless (Keypour et al. 2023; Truong et al. 2024). In general, NaBH_4 , a reducing agent, is decomposed as H_2 , diborane, and electrons. H_2 and electrons are captured by the catalyst (Mascarenhas and Varanda 2021). Then, adsorption of the H_2 molecule and subsequent dissociation onto the Bi NPs surface occurs. Bi NPs produce partly charged H_2 species on their surface by functioning as an electron relay. MO molecules are adsorbed to the surface of the catalyst. The adsorbed MO molecules are reduced

Fig. 7 The possible decolorization mechanism of MO on Bi/HAp-rGO



via electron capture of the active sites of the catalyst along with H_2 species (Hata et al. 2022, Mascarenhas and Varanda 2021).

Conclusion

The optimization and modeling of MO decolorization in the presence of $NaBH_4$ were applied experimentally via RSM-CCD. An easy approach was developed to produce a Bi/HAp-rGO as a catalyst for the decolorization of MO. The functional relation among the decolorization efficiency and four parameters (time, MO conc., $NaBH_4$ amount, and catalyst amount) was defined using the obtained quadratic model. The optimum conditions for MO decolorization were time 2.91 min, MO conc. 18.85 mg/L, $NaBH_4$ amount 18.35 mM, and Bi/HAp-rGO dosage 2.12 mg/mL. Almost all of the MO molecules were observed to be decolorized under the conditions obtained (99.6%). Lastly, a possible mechanism for decolorizing MO was put forth using Bi/HAp-rGO in the presence of $NaBH_4$. To summarize, it can be said that Bi/HAp-rGO shows great promise as a material for the highly effective removal of contaminants in water treatment.

Supplementary Information The online version contains supplementary material available at <https://doi.org/10.1007/s11356-024-33425-4>.

Author contribution Ümit Ecer: investigation, data analysis, material synthesis, characterization, and writing—reviewing and editing; Şakir Yılmaz: data analysis, experiments, methodology, material synthesis, characterization, writing, and reviewing; Berdan Ulaş: data analysis, methodology, material synthesis, characterization, writing, and reviewing; Serap Koç: investigation, material synthesis, characterization, and data analysis.

Funding Open access funding provided by the Scientific and Technological Research Council of Türkiye (TÜBİTAK).

Data availability The authors confirm that the data supporting the findings of this study are available within the article.

Declarations

Ethics approval The authors all agree to ethical approval and understand its related rules and content.

Consent to participate The authors of this manuscript are all aware of the journal to which the manuscript was submitted, and all agree to continue to support the follow-up work.

Consent for publication This manuscript has not been submitted or published in other journals, and the authors agree to consent to publish.

Competing interests The authors declare no competing interests.

Open Access This article is licensed under a Creative Commons Attribution 4.0 International License, which permits use, sharing, adaptation, distribution and reproduction in any medium or format, as long

as you give appropriate credit to the original author(s) and the source, provide a link to the Creative Commons licence, and indicate if changes were made. The images or other third party material in this article are included in the article's Creative Commons licence, unless indicated otherwise in a credit line to the material. If material is not included in the article's Creative Commons licence and your intended use is not permitted by statutory regulation or exceeds the permitted use, you will need to obtain permission directly from the copyright holder. To view a copy of this licence, visit <http://creativecommons.org/licenses/by/4.0/>.

References

- Acar MK, Altun T, Gubbuk IH (2023) Synthesis and characterization of silver doped magnetic clay nanocomposite for environmental applications through effective RhB degradation. *Int J Environ Sci Technol* 20:4219–4234
- Akl MA, Hashem MA, Mostafa AG (2023) Synthesis, characterization, antimicrobial and photocatalytic properties of nano-silver-doped flax fibers. *Polym Bull* 80:9745–9777
- Al-Amrani WA, Lim P-E, Seng C-E, Wan Ngah WS (2014) Factors affecting bio-decolorization of azo dyes and COD removal in anoxic-aerobic REACT operated sequencing batch reactor. *J Taiwan Inst Chem Eng* 45:609–616
- Al-Ansari SH, Gomaa H, Abdel-Rahim RD, Ali GAM, Nagiub AM (2024) Recycled gold-reduced graphene oxide nanocomposite for efficient adsorption and photocatalytic degradation of crystal violet. *Sci Rep* 14:4379
- Alovn D, Yazar S, Caglar A, Kivrak H (2023) Development of carbon nanotube-supported metal (Mo, Ga, Bi)-doped polyacrylic acid electrodes for supercapacitor applications. *J Electron Mater* 53:991–1001
- Alshaiqi HA, Asiri AM, Alamry KA, Marwani HM, Alfifi SY, Khan SB (2022) Copper nanoparticles decorated alginate/cobalt-doped cerium oxide composite beads for catalytic reduction and photodegradation of organic dyes. *Polymers* 14:4458
- Anwar Y, Mohammed Ali HSH, Rehman WU, Hemeg HA, Khan SA (2021) Antibacterial films of alginate-CoNi-coated cellulose paper stabilized Co NPs for dyes and nitrophenol degradation. *Polymers* 13:4122
- Bezerra MA, Santelli RE, Oliveira EP, Villar LS, Escalera LA (2008) Response surface methodology (RSM) as a tool for optimization in analytical chemistry. *Talanta* 76:965–977
- Bustos-Terrones YA, Hermosillo-Nevárez JJ, Ramírez-Pereda B, Vaca M, Rangel-Peraza JG, Bustos-Terrones V, Rojas-Valencia MN (2021) Removal of BB9 textile dye by biological, physical, chemical, and electrochemical treatments. *J Taiwan Inst Chem Eng* 121:29–37
- Ciobanu G, Harja M (2019) Cerium-doped hydroxyapatite/collagen coatings on titanium for bone implants. *Ceram Int* 45:2852–2857
- Ciobanu G, Bargan AM, Luca C (2015) New bismuth-substituted hydroxyapatite nanoparticles for bone tissue engineering. *JOM* 67:2534–2542
- Ding Y, Guo X, Kuang D, Hu X, Zhou Y, He Y, Zang Z (2021) Hollow Cu₂O nanospheres loaded with MoS₂/reduced graphene oxide nanosheets for ppb-level NO₂ detection at room temperature. *J Hazard Mater* 416:126218
- Ecer Ü, Yılmaz Ş (2024) Fabrication of magnetic biochar-MIL-68(Fe)-supported cobalt composite material toward the catalytic reduction performance of crystal violet. *J Water Process Eng* 57:104574
- Ecer Ü, Zengin A, Şahan T (2023) Fabrication and characterization of poly(tannic acid) coated magnetic clay decorated with cobalt

- nanoparticles for NaBH₄ hydrolysis: RSM-CCD based modeling and optimization. *Int J Hydrogen Energy* 48:23620–23632
- El-Aal MA, Ali HM, Ibrahim SM (2022) Cu-doped 1D hydroxyapatite as a highly active catalyst for the removal of 4-nitrophenol and dyes from water. *ACS Omega* 7:26777–26787
- El-Subruiti GM, Eltaweil AS, Sallam SA (2019) Synthesis of active MFe₂O₄/γ-Fe₂O₃ nanocomposites (metal = Ni or Co) for reduction of nitro-containing pollutants and methyl orange degradation. *NANO* 14:1950125
- Gungor Koc S (2019) Synthesis and characterization of strontium and chlorine co-doped tricalcium phosphate. *Mater Lett* 248:69–72
- Hanrahan G, Lu K (2006) Application of factorial and response surface methodology in modern experimental design and optimization. *Crit Rev Anal Chem* 36:141–151
- Hashemi Salehi M, Yousefi M, Hekmati M, Balali E (2019) Application of palladium nanoparticle-decorated Artemisia abrotanum extract-modified graphene oxide for highly active catalytic reduction of methylene blue, methyl orange and rhodamine B. *Appl Organomet Chem* 33:e5123
- Hata S, Sakai Y, Tani N, Kitano S, Habazaki H, Hirakawa A, Tanaka H, Inomata Y, Murayama T, Haruta M, Du Y, Shiraishi Y, Toshima N (2022) Pd–Rh alloyed nanoparticles on zeolite imidazolate framework-67 for methyl orange degradation. *ACS Appl Nano Mater* 5:16231–16241
- Januário EFD, Vidovix TB, Bergamasco R, Vieira AMS (2021) Performance of a hybrid coagulation/flocculation process followed by modified microfiltration membranes for the removal of solophenyl blue dye. *Chem Eng Process - Process Intensif* 168:108577
- Johra FT, Jung W-G (2015) Hydrothermally reduced graphene oxide as a supercapacitor. *Appl Surf Sci* 357:1911–1914
- Joseph S, Mathew B (2015) Facile synthesis of silver nanoparticles and their application in dye degradation. *Mater Sci Eng B* 195:90–97
- Joseph J, Radhakrishnan RC, Johnson JK, Joy SP, Thomas J (2020) Ion-exchange mediated removal of cationic dye-stuffs from water using ammonium phosphomolybdate. *Mater Chem Phys* 242:122488
- Keypour H, Kouhdareh J, Rabiei K, Karakaya İ, Karimi-Nami R, Alavinia S (2023) Pd nanoparticles decorated on a porous Co(BDC-NH₂) MOF as an effective heterogeneous catalyst for dye reduction. *Nanoscale Adv* 5:5570–5579
- Khalik W, Abd Rahman Azmi A, Mohd N (2020) Central composite design approach for the optimisation of catalytic degradation of methyl orange dye using silica-silver core-shell nanoparticles. *Res J Chem Environ* 24:104–111
- Khan N, Shahida B, Khan SA, Ahmad Z, Saeeduddin SZ, Bakhsh EM, Alraddadi HM, Fagieh TM, Khan SB (2023) Anchoring zero-valent Cu and Ni nanoparticles on carboxymethyl cellulose-polystyrene-block polyisoprene-block polystyrene composite films for nitrophenol reduction and dyes degradation. *J Polym Environ* 31:608–620
- Kurtan U, Amir M, Baykal A (2016) Fe₃O₄@Nico-Ag magnetically recyclable nanocatalyst for azo dyes reduction. *Appl Surf Sci* 363:66–73
- Lee JH, Shin YC, Lee S-M, Jin OS, Kang SH, Hong SW, Jeong C-M, Huh JB, Han D-W (2015) Enhanced osteogenesis by reduced graphene oxide/hydroxyapatite nanocomposites. *Sci Rep* 5:18833
- Liu X, Xu T, Li Y, Zang Z, Peng X, Wei H, Zha W, Wang F (2018) Enhanced X-ray photon response in solution-synthesized CsPbBr₃ nanoparticles wrapped by reduced graphene oxide. *Sol Energy Mater Sol Cells* 187:249–254
- Liu Y, Xiang Y, Xu H, Li H (2022) The reuse of nano-TiO₂ under different concentration of CO₃²⁻ using coagulation process and its photocatalytic ability in treatment of methyl orange. *Sep Purif Technol* 282:120152
- Liu X, Yang X, Xin H, Tang X, Weng L, Han Y, Geng D (2016) Ecofriendly fabrication of Au/Fe₃O₄-chitosan composites for catalytic reduction of methyl orange. *Dig J Nanomater Biostructures (DJNB)* 11:337–348
- Lu X, Zhu G, Zhang R, Li S, Pan L, Nie J, Rao F (2019) I-doped Bi₂WO₆ microflowers enhanced visible light photocatalytic activity for organic pollution degradation and NO removal. *J Mater Sci: Mater Electron* 30:17787–17797
- Mascarenhas BC, Varanda LC (2021) Catalytic hydrogenation of organic dyes by Ag nanoparticles on reduced graphene oxide. *J Ind Eng Chem* 103:124–135
- Najem M, Nada AA, Weber M, Sayegh S, Razzouk A, Salameh C, Eid C, Bechelany M (2020) Palladium/carbon nanofibers by combining atomic layer deposition and electrospinning for organic pollutant degradation. *Materials* 13:1947
- Naseem K, Begum R, Wu W, Irfan A, Al-Sehemi AG, Farooqi ZH (2019) Catalytic reduction of toxic dyes in the presence of silver nanoparticles impregnated core-shell composite microgels. *J Clean Prod* 211:855–864
- Osunlaja A, Idris S, Iyun J (2012) Kinetics and mechanism of the methylene blue-permanganate ion reaction in acidic medium. *Arch Appl Sci Res* 4:772–780
- Patel P, Maliekal PJ, Lingayat S, Badani PM (2022) Understanding the kinetics and reduction of methylene blue using NaBH₄. *Russ J Phys Chem B* 16:869–876
- Qin G, Zhang H, Liao H, Li Z, Tian J, Lin Y, Zhang D, Wu Q (2017) Novel graphene nanosheet-wrapped polyaniline rectangular-like nanotubes for flexible all-solid-state supercapacitors. *J Mater Sci* 52:10981–10992
- Rauf A, Sher Shah MSA, Choi GH, Humayoun UB, Yoon DH, Bae JW, Park J, Kim W-J, Yoo PJ (2015) Facile synthesis of hierarchically structured Bi₂S₃/Bi₂WO₆ photocatalysts for highly efficient reduction of Cr(VI). *ACS Sustain Chem Eng* 3:2847–2855
- Ravikumar KVG, Dubey S, Pulimi M, Chandrasekaran N, Mukherjee A (2016) Scale-up synthesis of zero-valent iron nanoparticles and their applications for synergistic degradation of pollutants with sodium borohydride. *J Mol Liq* 224:589–598
- Rogina A, Ivanković M, Ivanković H (2013) Preparation and characterization of nano-hydroxyapatite within chitosan matrix. *Mater Sc Eng: C* 33:4539–4544
- Roy S, Darabdhara J, Ahmaruzzaman M (2023) MoS₂ Nanosheets@Metal organic framework nanocomposite for enhanced visible light degradation and reduction of hazardous organic contaminants. *J Clean Prod* 430:139517
- Saikia P, Miah AT, Das PP (2017) Highly efficient catalytic reductive degradation of various organic dyes by Au/CeO₂-TiO₂nanohybrid. *J Chem Sci* 129:81–93
- Sarkar M, Denrah S, Patra M, Basu T (2021) Studies on the antibacterial and catalytic activities of silver nanoparticles synthesized from *Cyperus rotundus* L. *J Cluster Sci* 32:265–278
- Sen TK, Afroz S, Ang HM (2011) Equilibrium, kinetics and mechanism of removal of methylene blue from aqueous solution by adsorption onto pine cone biomass of *Pinus radiata*. *Water Air Soil Pollut* 218:499–515
- Sharma N, Sharma V, Vyas R, Kumari M, Kaushal A, Gupta R, Sharma SK, Sachdev K (2019) A new sustainable green protocol for production of reduced graphene oxide and its gas sensing properties. *J Sci: Adv Mater Devices* 4:473–482
- Sharma SK, Ranjani P, Mamane H, Kumar R (2023) Preparation of graphene oxide-doped silica aerogel using supercritical method for efficient removal of emerging pollutants from wastewater. *Sci Rep* 13:16448
- Shrivastava K, Dangi SS, Nema A, Bano M, Rai M, Verma V, Khan F (2024) Silver nanoparticle incorporated calcium crosslinked

- hydrogel composite for reduction of methylene blue dye and nitrite sensing. *J Photochem Photobiol A* 447:115256
- Song Q, Wang C, Wen S (2001) Effects of doping on crystal and grain boundary in human enamel. *Mater Sci Eng: A* 297:272–280
- Srivastava A, Rani R, Kumar S (2022) Optimization, kinetics, and thermodynamics aspects in the biodegradation of reactive black 5 (RB5) dye from textile wastewater using isolated bacterial strain, *Bacillus albus* DD1. *Water Sci Technol* 86:610–624
- Topçu E, Dağcı Kıranşan K (2019) Flexible gold nanoparticles/rGO and thin film/rGO papers: novel electrocatalysts for hydrogen evolution reaction. *J Chem Technol Biotechnol* 94:3895–3904
- Truong TBT, Nguyen TTT, Nguyen PA, Do BL, Van Nguyen TT, Huynh KPH, Phan HP, Dang-Bao T, Ho TG-T, Nguyen T (2024) Green synthesised nanocopper/chitosan aerogel biocomposite as a recyclable and nonprecious catalyst for methyl orange reduction. *Colloids Surf A* 680:132622
- Wang L, Cui Z-L, Zhang Z-K (2007) Bi nanoparticles and Bi₂O₃ nanorods formed by thermal plasma and heat treatment. *Surf Coat Technol* 201:5330–5332
- Wang Y, He L, Li Y, Jing L, Wang J, Li X (2020) Ag NPs supported on the magnetic Al-MOF/PDA as nanocatalyst for the removal of organic pollutants in water. *J Alloy Compd* 828:154340
- Wei J, Zang Z, Zhang Y, Wang M, Du J, Tang X (2017) Enhanced performance of light-controlled conductive switching in hybrid cuprous oxide/reduced graphene oxide (Cu₂O/rGO) nanocomposites. *Opt Lett* 42:911–914
- Xue X, Zhang J, Li M, Ao C, Wang Q, Zhao J, Zhang W, Lu C (2023) Facile fabrication of three-dimensional nanofibrous foams of cellulose@g-C₃N₄@Cu₂O with superior visible-light photocatalytic performance. *Carbohydr Polym* 303:120455
- Zhang J, Xu Y, Liu Z, Yang W, Liu J (2015) A highly conductive porous graphene electrode prepared via in situ reduction of graphene oxide using Cu nanoparticles for the fabrication of high performance supercapacitors. *RSC Adv* 5:54275–54282
- Zhou F, He D, Ren G, Yarahmadi H (2024) In situ and bio-green synthesis of silver nanoparticles immobilized on zeolite as a recyclable catalyst for the degradation of OPDs. *Sci Rep* 14:1143
- Zolfaghari S, Sharafadini R, Ghaedi M, Javadian H, Shokrollahi A, Shahvandi SK, Rodrigues VHN, Razmjoue D (2023) Synthesis of a coordination polymer based on Zn(DMF)(Tp) as a novel adsorbent for the simultaneous removal of quinoline yellow and azure B. *J Mol Struct* 1294:136572

Publisher's Note Springer Nature remains neutral with regard to jurisdictional claims in published maps and institutional affiliations.